

# CHAPTER 6. ELECTROCHEMICAL OSCILLATIONS IN METHANOL OXIDATION

## 6.1 Introduction

Based on the previous three experimental chapters dealing with the electrocatalytic oxidation of CO and HCOOH, dynamical instabilities in methanol oxidation (in which CO and also HCOOH can form as intermediate) are now presented. Although the oxidation mechanism of methanol is more complex and difficult to understand compared with CO and HCOOH, it is more interesting for technical applications, since methanol can be applied for direct methanol fuel cells.

As already demonstrated in Chapter 1, there has been a resurgence of interest in the studies of the oscillatory behaviour in electrochemical systems as electrocatalysis, electrodeposition, and electro-dissolution [14 – 17, 23, 24, 40, 58, 176].

In electrocatalysis, the most studied system with regard to the dynamic behaviour of small organic molecules is formic acid (HCOOH). Current oscillations under potentiostatic conditions and potential oscillations in galvanostatic systems of HCOOH on a Pt electrode were well investigated [22, 40, 53]. However, only a few studies of potential oscillations during anodic CH<sub>3</sub>OH oxidation were reported [56, 177, 178]. Pavela reported that diffusion of CH<sub>3</sub>OH might be the reason for the potential oscillations [177]. In the early 1960s, Buck *et al.* [178] observed only small potential oscillations in the CH<sub>3</sub>OH oxidation. Krausa and Vielstich [56] studied the experimental conditions of potential oscillations during CH<sub>3</sub>OH oxidation on a Pt electrode and they suggested a reaction mechanism resulting in different types of oscillations. The investigation of the oxidation mechanism of CH<sub>3</sub>OH and HCOOH on a Pt electrode has attracted attention, since the understanding of the oxidation of C<sub>1</sub> fuels can be applied for the development of clean energy techniques (fuel cell). While the temporal as well as spatiotemporal behaviour of HCOOH oxidation has been studied in

detail both experimentally and theoretically, the mechanistic origin of bistability and oscillations in  $\text{CH}_3\text{OH}$  oxidation is not well understood [23, 144 179 – 182].

First of all, we will try to categorise the mechanistic origin of the  $\text{CH}_3\text{OH}$  oxidation both on pure Pt and on Ru-modified Pt surface by electrochemical impedance spectroscopy (EIS) and the bifurcation sequence under galvanostatic conditions. Secondly, current oscillations under potentiostatic conditions with an appropriate external resistance ( $R_{\text{ex}}$ ) will be reported. This study could also be considered as a reference to understand the electrocatalytic oxidation of  $\text{C}_2$  and  $\text{C}_3$  compounds such as ethanol and propanol [183, 184] and can give important clues to obtain a higher power output under oscillatory conditions.

## 6.2 Experiments

The schematic diagram of the principal three-electrode arrangement is the same as that in Chapter 4. The electrochemical cell consisted of a glass cylinder (Duran) capped with a Teflon lid holding all three-electrodes. A smooth polycrystalline Pt ring of 34.5 mm inner diameter and 42.5 mm outer diameter cut from a Pt plate of 0.1 mm thickness, thus exhibiting a geometric surface area of  $10 \text{ cm}^2$ , was used as the working electrode (WE).

Pre-treatment of the working ring electrode is exactly the same as that in Chapter 4. After this preliminary check of the Pt electrode, WE was mounted in the Teflon lid of the cell which already held both the  $\text{Hg}/\text{Hg}_2\text{SO}_4$ , saturated  $\text{K}_2\text{SO}_4$  reference electrode and the platinized Pt counter electrode (see Figure 6.1). Two different concentrations of methanol, 0.03 M  $\text{CH}_3\text{OH}$  (Merck, p.a.) in 0.1 M  $\text{HClO}_4$  (Merck, suprapur) and 0.1 M  $\text{CH}_3\text{OH}$  (Merck, p.a.) in 0.1 M  $\text{HClO}_4$  (Merck, suprapur) were used and the electrolyte was extensively bubbled with  $\text{N}_2$  before each experiment. A nitrogen atmosphere was maintained over the unstirred solutions during sweep experiments.

Cyclic voltammetry, galvanostatic scan and constant current methods were executed with an in-house-built potentiostat (*ELAB* of Fritz-Haber-Institut) and a bi-Potentiostat (EG&G, Model 366). The impedance spectrum was measured by a frequency response analyser (S-5720, NF Electronic Instruments, Yokohama). The

frequency ranges from 10 kHz to 0.1 Hz were digitally recorded with 25 points per decade.

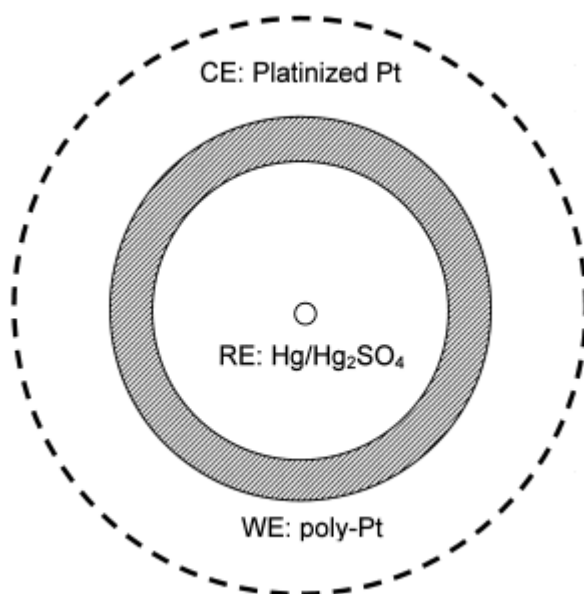


Figure 6.1. Experimental setup of three-electrode systems (2D plot) for the measurement of methanol oxidation.

### 6.3 Mechanistic classification of CH<sub>3</sub>OH oxidation on pure Pt

Figure 6.2 shows the typical current-potential profile in the CH<sub>3</sub>OH oxidation on unmodified Pt electrode. On the anodic scan, the adsorption of CH<sub>3</sub>OH and dehydrogenation of methanol result in the formation of CO–Pt at low overpotential that is marked with (a) in Figure 6.2. We observed an anodic current peak around *ca.* +50 mV, where surface water might react with adsorbed CO on a Pt electrode and produce CO<sub>2</sub>, proton (H<sup>+</sup>), electron (e<sup>-</sup>) and vacant site (\*) on the Pt surface. With increasing anodic potential, the current decreases due to the formation of hydroxide on the Pt surface. On the cathodic scan, the desorption of OH–Pt results in a burst of anodic current at +150 mV and the oxidation of CH<sub>3</sub>OH follows. We assume that the

current plateau marked with (b) in Figure 6.2 may be associated with next galvanostatic potential oscillations, but the detailed reaction mechanism is still unclear.

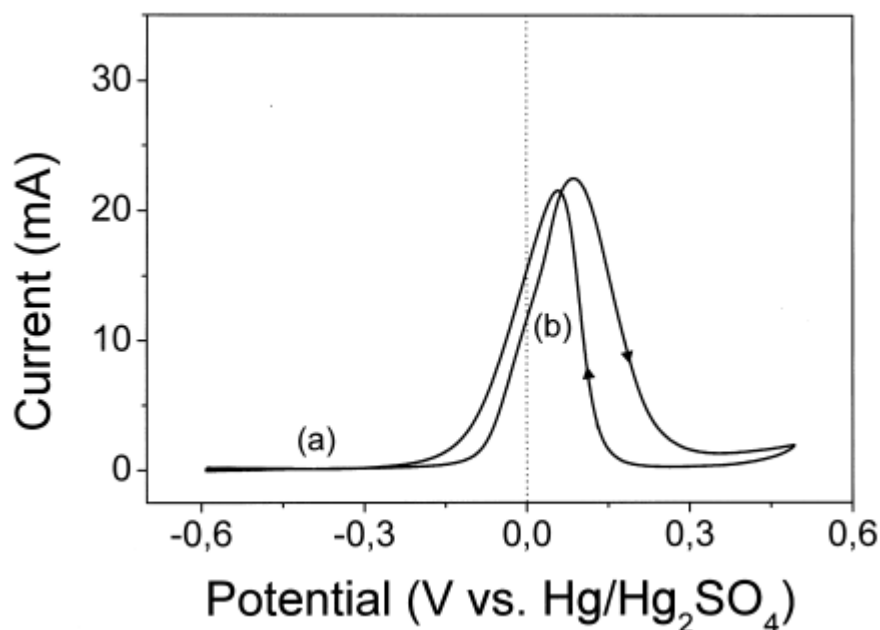


Figure 6.2. Cyclic voltammetry at a Pt electrode with a scan rate of 10 mV/s in 0.03 M  $\text{CH}_3\text{OH}/0.1$  M  $\text{HClO}_4$  solution.

Figure 6.3 shows the galvanostatic scan of  $\text{CH}_3\text{OH}$  oxidation on a Pt electrode. Current scan rate is  $+25 \mu\text{A/s}$ . A hard transition marked with **HT** from oscillatory to stationary behaviour is seen at high current of *ca.*  $+20$  mA, while a soft supercritical Hopf bifurcation (**ST**) is discerned at low current. This measurement reveals an onset potential of spontaneous sustained oscillations between  $+45$  mV and  $+65$  mV. The value of the anodic current of oscillation initiation is about  $+17$  mA. According to previous mechanistic classifications [140, 144], we conclude that the origin of potential oscillations in  $\text{CH}_3\text{OH}$  oxidation belongs to class IV, *i.e.*, hidden-negative differential resistance (HNDR). The bifurcation behaviour further indicated that either class IV.1 or IV.2, IV.3 can be excluded [140, 144].

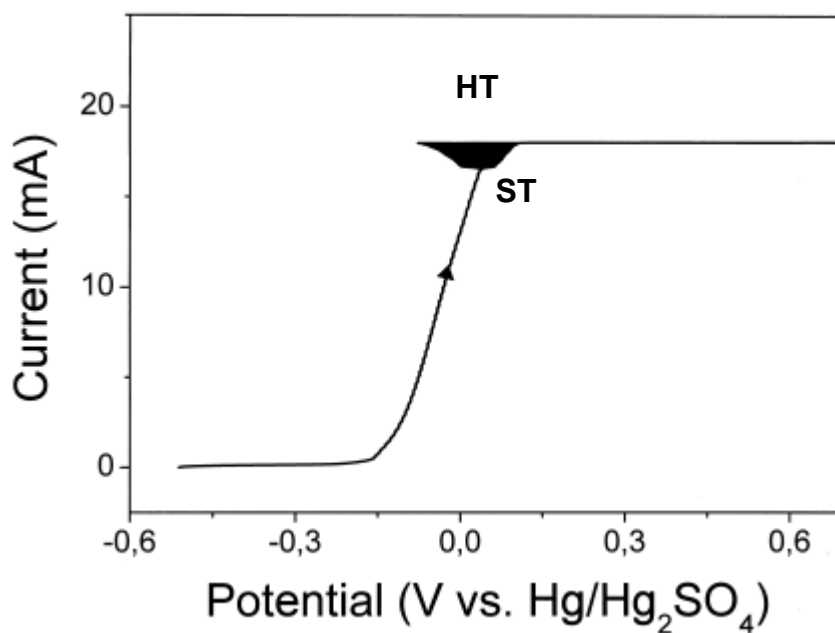


Figure 6.3. Onset of sustained potential oscillations (indicating Hopf bifurcation) in the galvanostatic operation mode (current-potential plot) with a scan rate of  $25 \mu\text{A/s}$  in  $0.03 \text{ M CH}_3\text{OH}/0.1 \text{ M HClO}_4$ .

To prove the mechanistic origin of oscillations in  $\text{CH}_3\text{OH}$  oxidation on a Pt electrode classified as HNDR, impedance spectra were measured for various potentiostatic operation points prior to the onset of periodic instabilities. Electrochemical impedance spectroscopy is a common tool to investigate the kinetics of electrochemical processes over a large range of frequencies (cf. sub-section 2.1.2). This makes it an ideal predictive technique to probe electrochemical systems for their ability to exhibit dynamical instabilities. Nyquist plots at three different applied outer potentials ( $U$ ) and a Bode plot at  $+65 \text{ mV}$  are shown in Figure 6.4. At an outer potential of  $+45 \text{ mV}$  (Figure 6.4(a)), the impedance plot  $Z(\omega)$  exhibits a clockwise capacitive-inductive loop indicating dynamically stable stationary operating points.

However, the impedance plot is drastically changed at higher overpotential  $+65 \text{ mV}$ , as shown in Figure 6.4(b).  $Z(\omega)$  wraps around the origin counter-clockwise. The intersection of the impedance and the negative real axis is obtained at a finite frequency,  $\omega_0 \approx 1 \text{ Hz}$ . Then  $Z(\omega)$  again exhibits positive real resistances for very low frequencies (see Figure 6.4(b) and (c)). The detailed shape of the Nyquist plot bears information on the mechanistic origin of the oscillatory behaviour, which can be used to predict the dynamical stability of oscillatory systems.

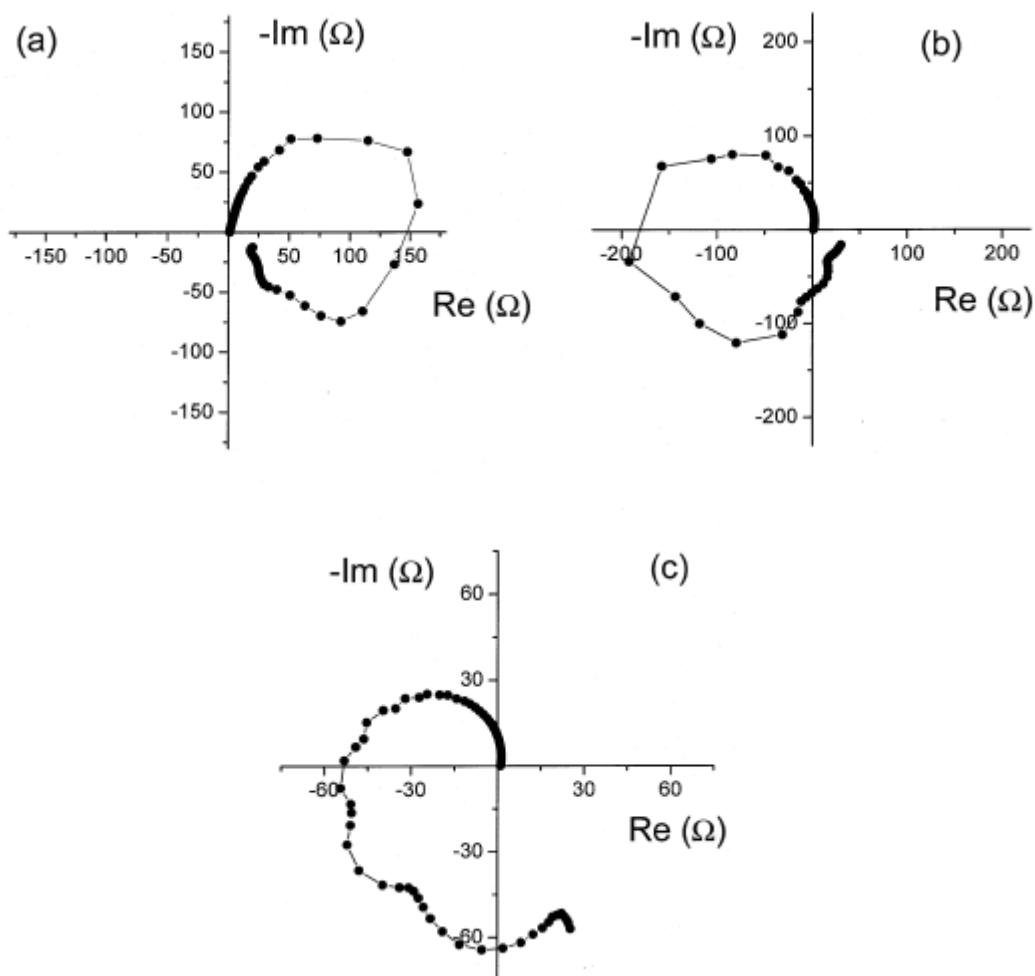


Figure 6.4. Electrochemical impedance behaviour of methanol oxidation on a Pt electrode measured at three outer potentials of (a) + 45 mV, (b) + 65 mV and (c) + 85 mV (numbers indicate the frequency).

Figure 6.5 is the Bode plot at + 65 mV and it clearly demonstrates that the phase angle jumps from  $-180^\circ$  to  $+180^\circ$  (see dotted circle in Figure 6.5), at a frequency  $\omega_0 = ca. 1 \text{ Hz}$ ; *i.e.*, this drastic phase change results in an anti-clockwise impedance profile in the Nyquist plot (Figures 6.4(b) and 6.4(c)).

Figures 6.6(a) and 6.6(b) show the potential oscillations at constant anodic current of + 14.5 mA at different times. It was measured without applying any forced convection such as stirring or nitrogen bubbling. Note that the value of  $\omega_0$  in the impedance spectra (see Figures 6.4(b) and 6.4(c)), the intersection where  $\text{Im } Z = 0$  with  $\text{Re } Z < 0$ , agrees with the initial oscillation frequency of 1 Hz obtained in Figure 6.6. As

discussed in previous work [30, 140], the critical potential, where the Nyquist plot blows up such that it approaches  $\pm$  infinity, marks the galvanostatic transition to periodic behaviour, *i.e.*, Hopf bifurcation. The value of  $\omega_0$  represents the intrinsic frequency of the oscillation in the electrocatalytic oxidation of  $\text{CH}_3\text{OH}$  on pure Pt.

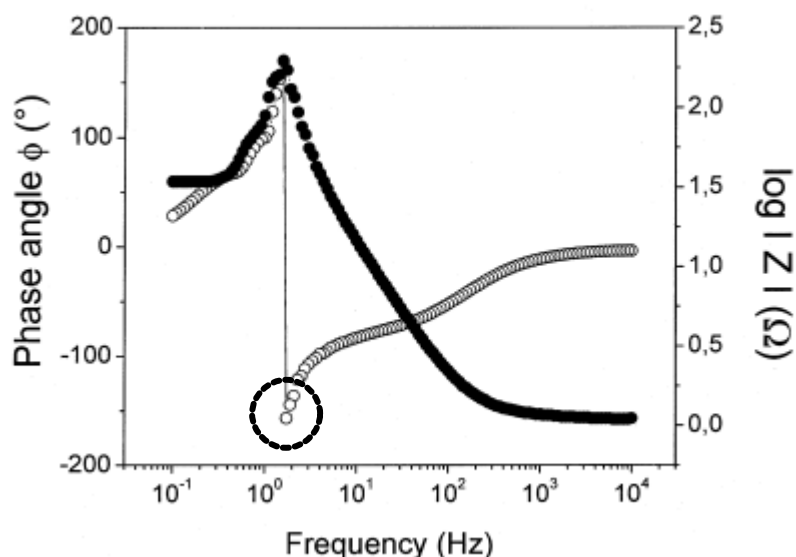


Figure 6.5. The Bode plot at + 65 mV shows the phase shift as a function of frequency. Experimental condition is as in Figure 6.2. Closed and open circles indicate  $\log |Z|$  and phase angle, respectively.

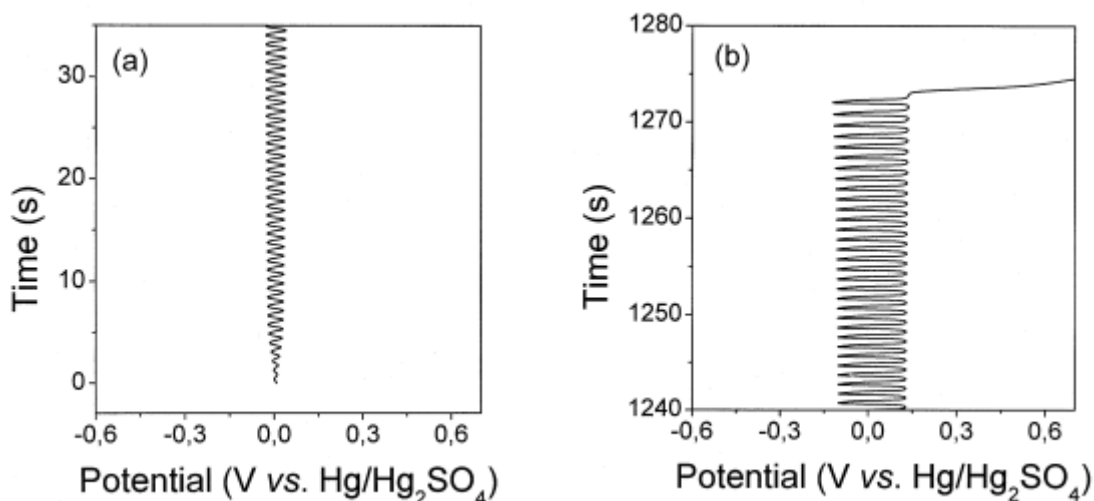
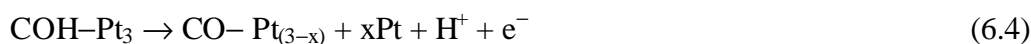
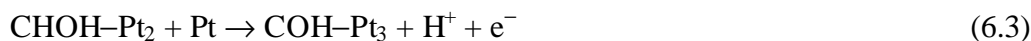
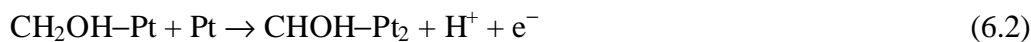


Figure 6.6. Potential oscillations at a constant current of + 14.5 mA show an oscillation frequency of 1 Hz. It is in good agreement with the result obtained in Figures 6.4(b) and 6.4(c). (a) Soft transition (ST) and (b) hard transition (HT).

According to previous work [185], a stepwise dehydrogenation mechanism for the oxidation of methanol is formulated as follows:



After applying an anodic current, the surface will be covered by  $\text{CH}_3\text{OH}$  residues with different oxidation states. If reaction rates of dehydrogenation from (6.1) to (6.4) are slow, only few vacant Pt sites remain and, thus, further dehydrogenation or oxidation of the  $\text{CH}_3\text{OH}$  residues is slowed down further. Therefore, the adsorption of  $\text{H}_2\text{O}$  must be considered (Eq. (6.5)) for the complete oxidation of  $\text{CH}_3\text{OH}$  as shown in Eq. (6.6), since  $\text{H}_2\text{O}$  is the source of oxygen. However, this adsorption process also needs free Pt sites. Thus, the potential rises until greater amounts of  $\text{OH-Pt}$  are formed and more free Pt sites are present by the autocatalytic reaction (see Eq. (6.6)) of the oxidation of  $\text{CO-Pt}$ , and the conversion of the residues can proceed with a higher reaction rate. During this reaction the potential will decrease slowly until larger areas of the surface are empty, then the potential decreases rapidly for about +200 mV in a negative direction.

## 6.4 CH<sub>3</sub>OH oxidation on a Ru-modified Pt surface

As already described in Chapter 4 and section 6.3, there are many examples of systems that exhibit spontaneous potential oscillations under galvanostatic control. Although not in quite the same way as the systems discussed in the previous study, these systems can also oscillate under potentiostatic control in the presence of a series resistance. Thus, it is not entirely accurate to classify these two systems according to the type of electrical control under which they may exhibit oscillations. Having discussed the origin of the oscillations in a typical galvanostatic oscillator in this section, a more precise criterion to distinguish between the two classes of electrochemical oscillators can be formulated. A typical example of a system which exhibits potential oscillations under galvanostatic control is the electrocatalytic oxidation of small organic molecules, such as methanol, formaldehyde and formic acid, at transition metals such as Pt, rhodium or iridium. This section looks into kinetic instabilities in methanol oxidation on Ru-modified Pt by means of impedance spectroscopy.

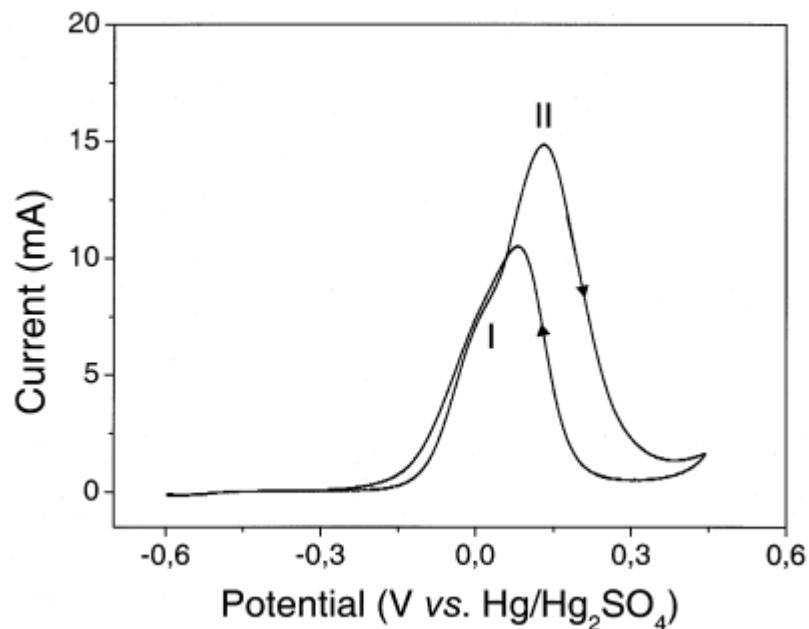


Figure 6.7. Cyclic voltammetry on Ru/Pt electrode with a scan rate of 10 mV/s in 0.1 M CH<sub>3</sub>OH/0.1 M HClO<sub>4</sub> solution. Current plateau around 0 V on the positive going scan is obtained [186].

The deposition of ruthenium (Ru) was carried out in 5 mM  $\text{RuCl}_3 \cdot x\text{H}_2\text{O}$  (Aldrich, 99.999 %)/0.1 M  $\text{H}_2\text{SO}_4$  (Merck, suprapur) for 2 min at open circuit potential of +0.04 V (*vs.*  $\text{Hg}/\text{Hg}_2\text{SO}_4$ ). During the deposition of Ru, magnetic stirring was applied for the uniform distribution of deposited Ru on the Pt surface.

Figure 6.7 shows the current-potential curve during methanol oxidation on a Pt electrode modified by Ru nanoparticle. Since oxygen could be formed on a Ru surface at the pronounced anodic peak, marked with **I** on the positive scan, the oxidation of methanol sets in at *ca.* 150 mV lower outer potential compared with that on unmodified Pt (see Figure. 6.2). In other words, the role of deposited Ru is the decrease of the oxidation potential of poisoning intermediate (CO) in methanol oxidation compared with pure Pt. Adsorbed CO on Pt is oxidised to  $\text{CO}_2$  by reacting with OH on the Ru surface (see Eq. (6.7))

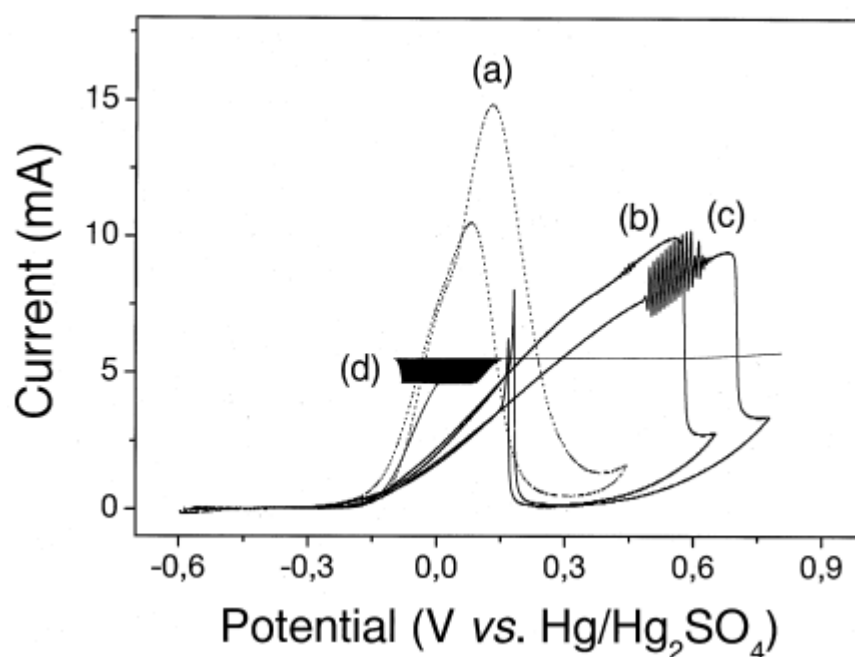
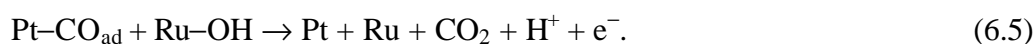


Figure 6.8. Cyclic voltammetry of 0.1 M  $\text{CH}_3\text{OH}$  in 0.1 M  $\text{HClO}_4$  solution on a Ru/Pt electrode with applying external resistance, (a)  $0\ \Omega$ , (b)  $45\ \Omega$  and (c)  $60\ \Omega$ . Scan rate is 10 mV/s and without any external force such as magnetic stirring, rotating electrode and gas bubbling. (d) Galvanostatic potential oscillations with a scan rate of 20  $\mu\text{A}/\text{s}$  [186].

Figure 6.8 gives the CV of 0.1 M  $\text{CH}_3\text{OH}$  in 0.1 M  $\text{HClO}_4$  at Ru/Pt. Figure 6.8(a) is the CV in the absence of an external resistance ( $R_{\text{ex}}$ ). With applying an external resistance, current oscillations appear on the positive scan, as is illustrated by the curves labeled 45  $\Omega$  (Figure 6.8(b)) and in 60  $\Omega$  (Figure 6.8(c)). Although there is a non-zero electrolyte resistance, it is not sufficiently large to induce oscillations. Under galvanostatic control, potential oscillations are observed as shown in Figure 6.8(d). Note that the potential oscillations occur around a branch of the polarization curve with positive slope. If one measures the impedance spectroscopy under stable potentiostatic conditions in that potential region, one observes the curves shown in Figure 6.9.

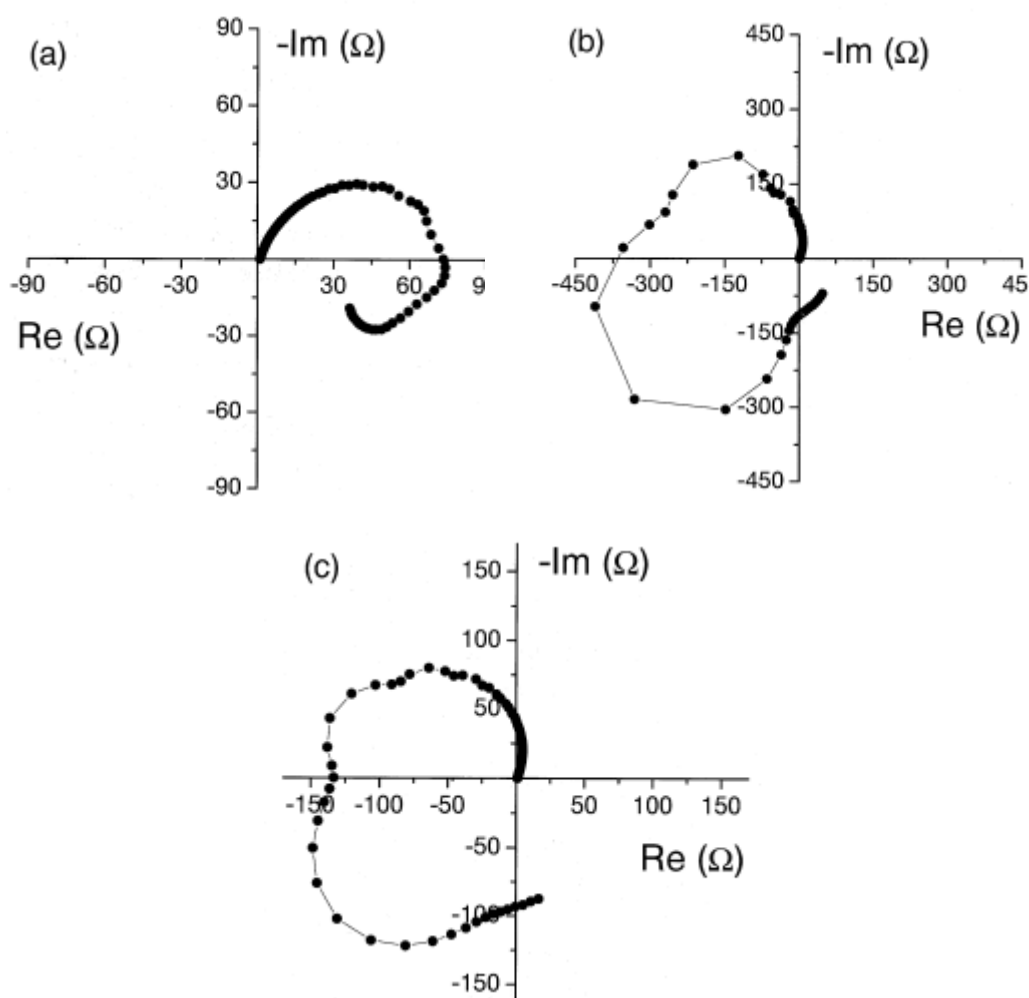


Figure 6.9. Impedance diagram taken at  $-65 \text{ mV}$ ,  $-5 \text{ mV}$  and  $+20 \text{ mV}$ . Electrolyte is 0.1 M  $\text{CH}_3\text{OH}$  in 0.1 M  $\text{HClO}_4$  solution on a Ru/Pt electrode in the absence of external resistance ( $0 \Omega$ ). Scan rate is 10 mV/s.

Figure 6.9(a) with the closed circles, taken at outer potential of  $-65$  mV, is a typical clockwise capacitive-inductive loop. On the other hand, the impedance curve at  $-5$  mV exhibits a negative impedance for a range of non-zero frequencies, but is positive for the lowest frequencies, in accordance with the positive polarization slope. From the theory described in a previous study [187] on stability and impedance spectroscopy, one can deduce that such a spectrum will lead to an oscillatory instability under galvanostatic control. The negative impedance is in some sense **hidden**, as it cannot be detected from the polarization curve, but does lead to the oscillations observed in the presence of correct external resistance. The curve should be contrasted with the data obtained during  $\text{H}_2\text{O}_2$  reduction [125], which is typical for a system that oscillates only under potentiostatic conditions but not under galvanostatic conditions. Note that the curves labelled (b) and (c) in Figure 6.8 are very similar to the curve in electrochemical dissolution of Ni. In fact, the sudden drop in current, which accompanies the extinction of the oscillations on the anodic scans, is a monoclinic bifurcation. The monoclinic bifurcation could also be found during the Galvan static scan in which a sudden transition (**HT**) to very high positive potentials occurs. This monoclinic bifurcation is in fact typical for systems with a hidden negative impedance.

## 6.5 Discussion

The occurrence of HNDR type oscillations as described above might play a crucial role in the operation of fuel cells, as will be described below.

### 6.5.1 Theoretical energy losses due to entropy production

To begin with, dissipation (energy loss) could be defined as in Eq. (6.6) according to Gibbs's law. Efficiency is power output ( $P_{\text{out}}$ ) divided by power input ( $P_{\text{in}}$ ) and, thus, dissipation could also be defined as the difference between  $P_{\text{in}}$  and  $P_{\text{out}}$  (see Eq. (6.8)). Now energy efficiency ( $\eta$ ) by using normalised dissipation ( $D'$ ) will be discussed.

$$\text{Dissipation} \quad D = T \frac{dS}{dt} \quad (6.6)$$

$$\text{Efficiency} \quad \eta = \frac{P_{\text{out}}}{P_{\text{in}}} \quad (\text{P: power}) \quad (6.7)$$

$$\text{Dissipation} \quad D = P_{\text{in}} - P_{\text{out}} \quad (6.8)$$

$$\text{Normalise} \quad \eta = 1 - D' \quad (D' = \frac{D}{P_{\text{in}}}). \quad (6.9)$$

### Isothermal systems

In isothermal systems, the dissipation is equal to the Flux multiplied by the driving Force which are current and overvoltage in electrical systems.

$$D = \text{Flux} \times \text{Force} = \text{Reaction rate} \times \text{Affinity (chemical)}$$

$$\text{Current} \times \text{Voltage (electrical).}$$

### Time-periodic processes

In time-periodic processes, the difference ( $\Delta D$ ) between the average value of dissipation ( $\langle D \rangle$ ) under oscillatory conditions with period of  $2\pi/\omega$  and dissipation at stationary systems ( $D_{\text{stationary}}$ ) can be calculated through Eq. (6.11) to (6.12). Here negative difference of dissipation is thermodynamically needed for obtaining higher energy efficiency.

$$\langle D \rangle = \frac{\omega}{2\pi} \int_0^{\frac{2\pi}{\omega}} D(t) dt \quad \text{period } \frac{2\pi}{\omega} \quad (6.10)$$

$$\Delta D = \langle D \rangle - D_{\text{stationary}} \quad (6.11)$$

$$\Delta D < 0 \text{ is required.} \quad (6.12)$$

## 6.5.2 Power output under oscillatory conditions

### Linear thermodynamics

When a dynamical system is sufficiently close to equilibrium, there is a linear relationship between flux and driving force according to the following equation (6.13).

$$\text{Flux} = \text{constant} \times \text{Force}$$

$$I = 1/R \times U \text{ (Ohm's law)}. \quad (6.13)$$

Then we can calculate  $\Delta D$  under periodically perturbed conditions. In this case, flux and force are in phase.

$$U(t) = U_0 + \Delta U \cos \omega t, \quad (U: \text{outer overpotential}) \quad (6.14a)$$

$$I(t) = I_0 + \kappa \Delta U \cos \omega t \quad (\kappa: \text{conductivity}). \quad (6.14b)$$

According to the following mathematical reference,

$$\int \cos at \, dt = \frac{1}{a} \sin at, \quad \int \cos^2 at \, dt = \frac{1}{2}t + \frac{1}{4a} \sin 2at$$

$$\begin{aligned} \langle D \rangle &= \frac{\omega}{2\pi} \int_0^{\frac{\omega}{2\pi}} D(t) \, dt = \frac{\omega}{2\pi} \int_0^{\frac{\omega}{2\pi}} U(t) \times I(t) \, dt \\ &= \frac{\omega}{2\pi} \left( \int_0^{\frac{\omega}{2\pi}} U_0 \times I_0 \, dt + \int_0^{\frac{\omega}{2\pi}} U_0 \kappa \Delta U \cos \omega t \, dt + \right. \\ &\quad \left. \int_0^{\frac{\omega}{2\pi}} I_0 \kappa \Delta U \cos \omega t \, dt + \int_0^{\frac{\omega}{2\pi}} \kappa \Delta U^2 \cos^2 \omega t \, dt \right) \end{aligned}$$

$$\begin{aligned}
&= U_0 I_0 + \frac{\omega}{2\pi} \left| U_0 \kappa \Delta U \times \frac{1}{\omega} \sin \omega t \right|_0^{2\pi/\omega} + \frac{\omega}{2\pi} \left| I_0 \kappa \Delta U \times \frac{1}{\omega} \sin \omega t \right|_0^{2\pi/\omega} \\
&\quad + \frac{\omega}{2\pi} \kappa \Delta U^2 \left| \frac{1}{2} t + \frac{1}{4\omega} \sin \omega t \right|_0^{2\pi/\omega} \\
\langle D \rangle &= U_0 I_0 + \kappa \Delta U^2 \times \frac{\omega}{2\pi} \times \frac{2\pi}{\omega} \times \frac{1}{2} = U_0 I_0 + \frac{1}{2} \kappa \Delta U^2 \quad (6.15a)
\end{aligned}$$

$$D_{\text{stationary}} = U_0 \times I_0 \quad (6.15b)$$

$$\Delta D = \kappa \Delta U^2 \frac{\omega}{2\pi} \int_0^{\frac{2\pi}{\omega}} \cos^2 \omega t dt = \frac{1}{2} \kappa \Delta U^2 > 0. \quad (6.15c)$$

In linear thermodynamics,  $\Delta D$  is always bigger than zero, which means that the efficiency can only decrease in linear systems.

### Nonlinear systems

In nonlinear systems, autonomous oscillations and/or both externally driven oscillations can occur. In principle, the phase between flux and force could be anything from  $-\pi$  to  $+\pi$  and generally depends in the time scale. We can get  $\Delta D$  (see Eq. (6.16)) under nonlinear systems according to above mathematical calculations.

$$\Delta D = \kappa \Delta U^2 \frac{\omega}{2\pi} \int_0^{\frac{2\pi}{\omega}} \cos \omega t \cos(\omega t + \varphi) dt = \frac{1}{2} \kappa \Delta U^2 \cos \varphi. \quad (6.16)$$

Analysing above thermodynamical calculations under oscillatory conditions, there exist two limiting cases. The phase between flux and force can vary over a wide range in nonlinear systems. On the one hand, the phase may be close to zero, which corresponds to a linear system, as Eq. 6.15(c)). On the other hand, if the phase is  $+\pi$  or  $-\pi$  ( $-180^\circ$  or  $+180^\circ$ ) between flux (current) and force (potential),  $\Delta D$  has a

maximum negative value, that is, higher energy efficiency can be obtained by applying a periodic perturbation compared with stationary operating conditions. Moreover, autonomous oscillations of an HNDR electrochemical system exhibit just this phase relationship at the Hopf bifurcation and, thus, have a higher efficiency in the oscillatory state.

$$(a) \varphi \approx 0 \quad \text{as linear system} \quad (6.17a)$$

$$(b) \varphi \approx \pi \quad \Delta D = -\frac{1}{2} \kappa \Delta U^2. \quad (6.17b)$$

## 6.6 Summary

Electrochemical impedance spectroscopy and the galvanostatic scan of CH<sub>3</sub>OH oxidation on Pt and on Ru/Pt exhibit a hidden negative differential resistance (HNDR) and a Hopf bifurcation at low overpotential. Therefore, this oscillator belongs to class IV according to an earlier mechanistic classification [140, 144], as did HCOOH oxidation [23]. Compared with stationary conditions, higher efficiency of a direct C<sub>1</sub> fuel cell is theoretically possible in an oscillatory state. On the Ru/Pt surface, we observed current oscillations on the anodic scan with applying a sufficient external resistance. Thus, further studies should be carried out to get higher power output by either exploiting the autonomous oscillations or applying an external pulse with the correct frequency obtained by EIS.

